**Atmospheric
Chemistry
and Physics**

Iterative maximum a posteriori (IMAP)-DOAS for retrieval of strongly absorbing trace gases: Model studies for CH$_4$ and CO$_2$ retrieval from near infrared spectra of SCIAMACHY onboard ENVISAT

C. Frankenberg, U. Platt, and T. Wagner

Institute of Environmental Physics, Heidelberg, Germany

Abstract. In the past, differential optical absorption spectroscopy (DOAS) has mostly been employed for atmospheric trace gas retrieval in the UV/Vis spectral region. New spectrometers such as SCIAMACHY onboard ENVISAT also provide near infrared channels and thus allow for the detection of greenhouse gases like CH$_4$, CO$_2$, or N$_2$O. However, modifications of the classical DOAS algorithm are necessary to account for the idiosyncrasies of this spectral region, i.e. the temperature and pressure dependence of the high resolution absorption lines. Furthermore, understanding the sensitivity of the measurement of these high resolution, strong absorption lines by means of a non-ideal device, i.e. having finite spectral resolution, is of special importance. This applies not only in the NIR, but can also prove to be an issue for the UV/Vis spectral region.

This paper presents a modified iterative maximum a posteriori-DOAS (IMAP-DOAS) algorithm based on optimal estimation theory introduced to the remote sensing community by Rodgers (1976). This method directly iterates the vertical column densities of the absorbers of interest until the modeled total optical density fits the measurement. Although the discussion in this paper lays emphasis on satellite retrieval, the basic principles of the algorithm also hold for arbitrary measurement geometries.

This new approach is applied to modeled spectra based on a comprehensive set of atmospheric temperature and pressure profiles. This analysis reveals that the sensitivity of measurement strongly depends on the prevailing pressure-height. The IMAP-DOAS algorithm properly accounts for the sensitivity of measurement on pressure due to pressure broadening of the absorption lines. Thus, biases in the retrieved vertical columns that would arise in classical algorithms, are obviated. Here, we analyse and quantify these systematic biases

as well as errors due to variations in the temperature and pressure profiles, which is indispensable for the understanding of measurement precision and accuracy in the near infrared as well as for future intercomparisons of retrieval algorithms.

1 Introduction

Absorption spectroscopy in the UV/Vis spectral region has been widely and successfully employed as a method for determining total column densities of several trace gases in the atmosphere (cf. Platt, 1994; Wagner and Platt, 1998). Satellite borne measurement devices such as GOME or SCIAMACHY use solar radiation reflected from the earth's surface and scattered within the earth's atmosphere as light source.

In addition to UV/Vis channels, SCIAMACHY onboard ENVISAT provides 3 near infrared channels covering wavelengths from 1–1.75 μm, 1.94–2.04 μm and 2.26–2.38 μm with moderate spectral resolution (Bovensmann et al., 1999). Among the absorbers in these regions are the greenhouse gases CO$_2$, CH$_4$, N$_2$O and H$_2$O as well as CO. SCIAMACHY thereby paves the way for the first global measurements of tropospheric CO$_2$ and CH$_4$ from space. Since these greenhouse gases are longlived, their spatial and temporal variations are fairly low, posing the problem of measuring small deviations from a large background total column. Thus, high measurement precision is needed in order to gain information in addition to the existing sparse but precise ground based measurements (Tans et al., 1996; Rayner and O'Brien, 2001; Levin et al., 2002; Olsen and Randerson, 2004). Furthermore, the retrieval has to be bias-free which will be one of the main issues addressed in this paper.

Correspondence to: C. Frankenberg
(cfranken@iup.uni-heidelberg.de)

Some authors have already noticed the drawbacks of the classical DOAS algorithm under certain conditions. Maurellis et al. (2000) parameterised the DOAS algorithm for highly structured spectra, while Solomon et al. (1989) and Volkamer et al. (1998) analysed the interference between different absorbers. A more general approach was introduced by Buchwitz et al. (2000) in the form of a new weighting function based modified DOAS approach for retrieval in the near infrared. This work firstly implemented the use of linearisation points in the classical DOAS approach which is vitally important for the retrieval of strongly absorbing gases. Also Schrijver (1999) focussed on retrieval in the near infrared and first results from SCIAMACHY are available from both groups (Buchwitz et al., 2004a,b; Gloudemans et al., 2004). Especially for the precise retrieval of longlived gases, some progress has been made on quantifying the influence of clouds and aerosols on the retrieval (Buchwitz et al., 2000; O'Brien and Rayner, 2002; Rayner et al., 2002).

The major focus of this work is the general treatment of strong absorbers, interferences between different absorbers and the characteristic features of the near infrared spectral region, viz. the shape of the spectral absorption lines and how they determine the sensitivity of the measurement inspite of often not being fully resolved by the spectrometer. This issue is hence analyzed in conjunction with instrumental lineshape issues, in particular with respect to measurement devices having moderate spectral resolution. This encompasses the influence of the actual atmospheric state on the retrieval and the effect of the nonlinearity of the forward model. Till date, only few climatological profiles have been used in other studies to analyze this effect. Our study makes use of a comprehensive set of atmospheric profiles to cover a realistic set of atmospheric states.

2 Basic Theory

The classical DOAS approach (Platt, 1994) uses the Lambert-Beer law to obtain a linear system of equations where the column density to be retrieved is directly proportional to the measured differential optical density, i.e. to the high frequent part of the optical density:

$$I(\nu) = I_0(\nu) \exp\left(-\int \sigma(\nu, p, T) c(s) ds\right) \tag{1}$$

$$\tau = \ln\left(\frac{I_0(\nu)}{I(\nu)}\right) \approx \sigma(\nu, \bar{p}, \bar{T}) \cdot \int c(s) ds$$
$$= \sigma(\nu, \bar{p}, \bar{T}) \cdot S, \tag{2}$$

where S denotes the slant column density, which is defined as the path integral of the concentration of the respective absorber along the actual lightpath. The ratio of the slant column density S and the vertical column density (VCD or simply V, the integral of the concentration along the vertical

from the surface to the top of atmosphere) is called airmass factor (A) and depends on many factors such as measurement geometry, albedo, wavelength and concentration profile. Neglecting scattering, the airmass factor can be approximated by simple geometric considerations of the slant light path. If aerosols and clouds are absent, this is a reasonable approximation in the near infrared and assumed in this study. However, airmass factors calculated by means of a radiative transfer model taking consideration of multiple scattering, refraction and spherical geometry can be directly used in the IMAP-DOAS algorithm.

Since absorption in the NIR is only due to rotational and vibrational transitions, the respective absorption lines are rather narrow and strongly temperature and pressure dependent. Thus, the integral in Eq. (1) cannot be simplified since $\sigma(\nu, p, T)$ is not constant along the light path ds. The total vertical optical densities of the respective absorbers therefore have to be calculated as the sum of the vertical optical densities of several height layers, each having nearly constant pressure and temperature.

Except for longpath-systems with reasonably well defined T and P, the simplification of Eq. (1) is generally only a rough approximation and almost all cross sections of species measured show a certain T-dependence. This also holds for the UV/Vis, where we have electronic transitions as well but where this dependence often plays only a minor role in the DOAS retrieval. However, we have to distinguish between a temperature effect which changes also the line intensity and is thus also important for weak absorbers, and pressure broadening which alters merely the lineshape and is thus only important if we are dealing with strong absorbers. As will be shown later, the importance of the actual lineshape will increase with the nonlinearity of the problem. Since most DOAS measurements in the UV/Vis deal only with weak absorbers which can be described by a linear problem, these issues have largely been neglected in the past.

2.1 Spectral line shape

In the case of Local Thermodynamic Equilibrium the absorption cross section of a single transition line $\sigma_i(\nu)$ can be written as the product of the line intensity S_i (not to be confused with the slant column density) and a frequency dependent part determining the line shape $\Phi_i(\nu)$ (Thomas and Stamnes, 1999):

$$\sigma_i(\nu) = S_i \Phi_i(\nu). \tag{3}$$

The line shape is mainly determined by doppler (Gaussian shape) and pressure broadening (Lorentzian shape). If both processes are assumed to be independent of each other, the resulting Voigt profile is a convolution of a Gaussian and a Lorentzian line shape (Goody and Yung, 1989):

$$\Phi(a, b) = \frac{b}{\pi^{3/2} \gamma_D} \int_{-\infty}^{\infty} \frac{\exp(-t^2)}{(a-t)^2 + b^2} dt, \tag{4}$$

with b denoting the ratio of the Lorentzian and the Gaussian halfwidth γ_L/γ_D and a the distance from the line center in units of the Gaussian halfwidth ($a=(\nu-\nu_0)/\gamma_D$). The Lorentzian halfwidth, γ_L, is directly proportional to the pressure p while γ_D is independent of p. All parameters used in this study have been taken from the latest release of the HITRAN database (Rothman et al., 2003). The Voigt function is computed in an efficient way as demonstrated by Kuntz (1997).

The total absorption cross section of a single molecule $\sigma_{tot}(\nu)$, or simply $\sigma(\nu)$, considering all transitions can then be described as the sum of the cross sections of all individual transitions:

$$\sigma(\nu) = \sum_i \sigma_i(\nu). \tag{5}$$

Strictly speaking, Eq. (5) is only valid when each transition can be treated separately (i.e. as an isolated line). If lines of different transitions overlap, e.g. due to pressure broadening, the wave functions of different rotational energy levels are no longer independent and simple summation is no more valid, since Eqs. (3) and (4) were based on the assumption of independence of rotational levels (Goody and Yung, 1989). This effect, called line-mixing, can alter the line shape and thus also the sensitivity of the measurements (Strow and Reuter, 1988) as it has a narrowing effect on the linewidths. Apart from line-mixing, the behavior of the line wings of a single transition could differ from a classical Lorentz shape (Goody and Yung, 1989). This deviation from the classical Lorentz theory is more likely for vigorously interacting molecules such as H_2O with the known problems of continuum absorption (Clough et al., 1989; Ma and Tipping, 1999). However, Pine (1997) found deviations from the Voigt profile as well as line mixing in the ν_3 band of CH_4 at about 3300 nm (3000 cm^{-1}). Since line mixing leads to a narrowing of the absorption lines, it is supposed to decrease the sensitivity of the measurement. So far, these effects have been neglected for the model analysis of CO_2 and CH_4 presented in this paper and we use the Voigt profile throughout this study.

2.2 Instrumental line shape

For grating spectrometers such as SCIAMACHY, a convolution of the high resolution structure of the incoming light with the instrumental slit function constitutes the actually recorded spectra. Dealing with narrow lines exhibiting relatively strong absorptions (optical densities >0.1) and moderate spectral resolution of the spectrometer (in our case 0.2–1.5 nm) is a crucial aspect in the NIR spectral region: the actual shape of the absorption lines cannot be fully resolved by the spectrometer. In order to account for all spectral features, the transmission has to be calculated using a fine wavelength grid before convolution with the instrumental function. This convolution has to be performed in the intensity space. Hence, the direct convolution of the optical densities,

τ, or cross sections, often used as a reasonable approximation for weak absorbers in the DOAS approach, is inappropriate in this case:

$$< I_0 \exp(-\tau) > \neq < I_0 > \exp(< -\tau >), \tag{6}$$

where I_0 is the Fraunhofer spectrum and $< \cdot >$ denotes the convolution with the (normalised) instrumental function $\phi_I(\lambda)$:

$$< I(\lambda) > = \int_{-\infty}^{\infty} I(\lambda') \cdot \phi_I(\lambda - \lambda') d\lambda' \tag{7}$$

Hence, the convolution is applied only in the intensity space throughout this study.

2.3 Sensitivity of the measurement

Since convolution and logarithm are not associative and we are dealing with strong, non-resolved absorption lines, the sensitivity of the measurement with respect to a perturbation in τ decreases with increasing τ and Eq. (2) is not valid any more. Pressure broadening decreases the maximum values of τ and therefore increases the sensitivity. In other words, the line wings contribute most to the sensitivity of strong absorption lines. However, since the shape of the line wings is generally less well known and cannot be always treated as a Voigt shape (Goody and Yung, 1989), this uncertainty could introduce further errors.

In the case of a moderate spectral resolution, the measured optical density is thus no longer linearly dependent on the vertical column density of the respective absorbers. Ignoring scattering, the theoretically measured slant optical density of a single absorber can be written as

$$\tau_\lambda^{meas}(x) = -\ln\left(< \exp(-x \cdot A \cdot \tau_\lambda^{ref}) > \right). \tag{8}$$

where

x	=	retrieved scaling factor for V (V/V^{ref})
τ_λ^{ref}	=	total vertical optical density
A	=	Airmass factor (A=S/V) .

Figure 1 shows an idealized case, where the transmission through a medium with constant pressure and temperature and with a column density of $7 \cdot 10^{19}$ molec/cm^2 CH_4 is computed at two different pressures. In panels (b1) and (b2) the high resolution transmission as well as their convolution with the instrumental slit function is shown. The width of the slit function is far larger than the actual width of the absorption lines. One can see that the resulting apparent optical densities, which would theoretically be measured by an instrument with the given slit function, in Fig. 1c differ for both pressures although the column density is the same. The medium with higher ambient pressure clearly exhibits a stronger apparent optical density due to the broader absorption lines as shown in the cross sections in panels (a1) and (a2).
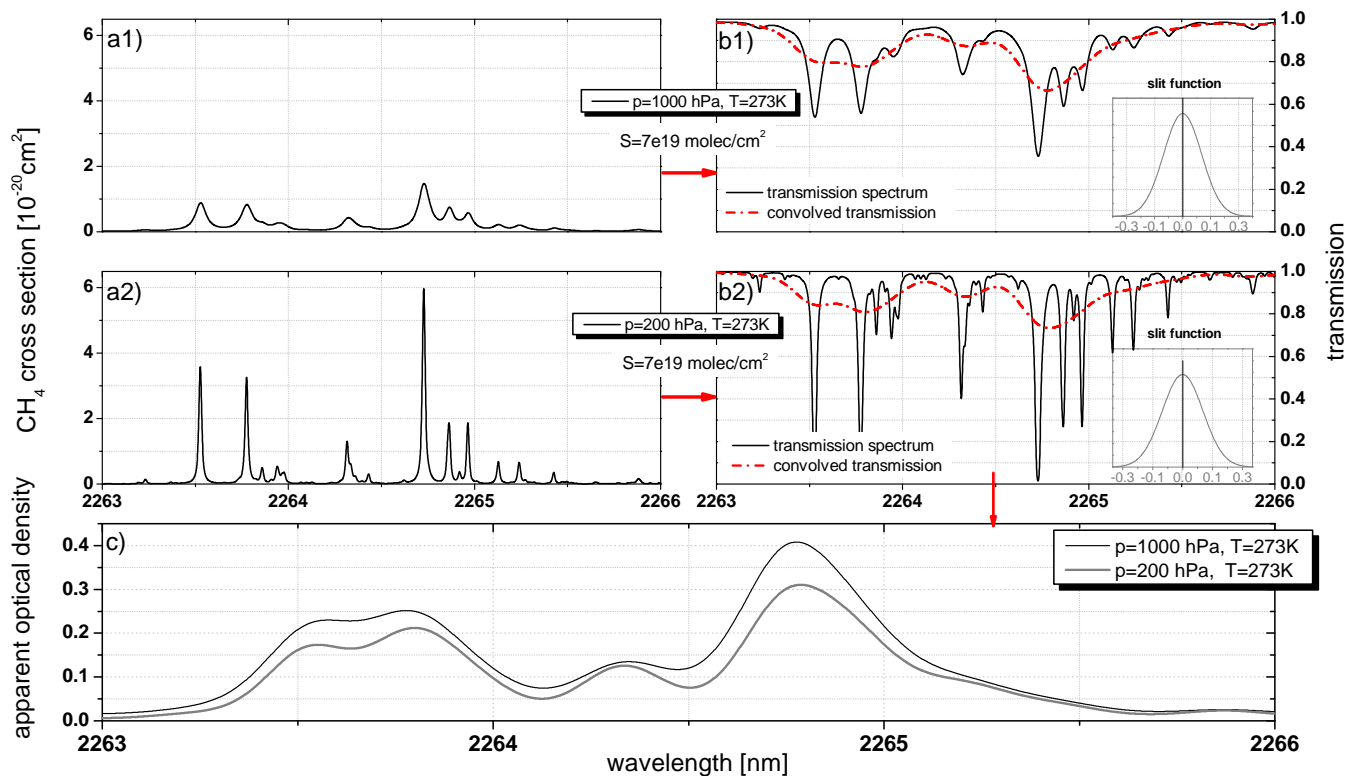
Fig. 1. Panel **(a1)** and **(a2)** show the cross sections of methane for two different ambient pressures. From these cross sections, the theoretical transmissions through a column of $7 \cdot 10^{19}$ molec/cm^2 CH$_4$ are depicted in panels **(b1)** and **(b2)**. Also shown are the convolutions of the high resolution transmission with the instrumental slit function (FWHM=0.24 nm). Panel **(c)** then shows the negative logarithm of the convolved transmissions.
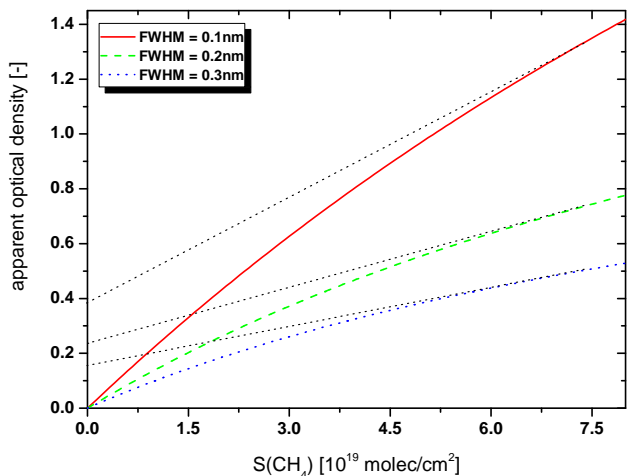
Fig. 2. Curve of growth for CH$_4$. Depicted is the apparent slant optical density at one single detector pixel (at about 2328 nm) due to CH$_4$ absorptions modeled with a gaussian slit function with different Full Width at Half Maximum. For the sake of simplicity, the air mass factor was chosen to be 2 (i.e. $S=2 \cdot V$). The weighting functions at S=7.5 molec/ cm^{-2} are indicated by the black, dotted lines (strictly speaking by the slope of these lines).

Assuming an inhomogeneous path, the total vertical optical density τ_λ^{ref} of the respective species is computed numerically from the integral $\tau_\lambda^{ref} = \int_0^{z_T} \sigma_\lambda \left(p(z), T(z) \right) c(z) dz$ where $c(z)$ is the volume number concentration of the respective species and z_T the top of atmosphere. In our algorithm, typically 40–60 height layers are chosen in order to account for the changes in temperature and pressure.

Figure 2 shows the theoretically measured (apparent) optical density due to CH$_4$ absorptions at a given wavelength where the (unconvolved) vertical optical density of methane is rather high (about 1.7 for a reference vertical column density of $3.6 \cdot 10^{19}$ molec/cm^{-2}). One can clearly see that the measured optical density is not linearly dependent on the slant column density of CH$_4$. Furthermore, the nonlinearity decreases with decreasing FWHM of the slit function but is still present even for a FWHM of 0.1 nm. The degree of nonlinearity also depends on the actual slant optical density itself. Thus, a classical DOAS approach which assumes strict linearity is not well applicable in the near infrared spectral region in particular and for strong absorbers in general.

2.4 Linearisation points and derivatives

Buchwitz et al. (2000) introduced the concept of weighting functions to the classical DOAS approach. The basic idea is to linearise the problem about a linearisation point in S, the expected slant column density derived using climatological profiles of meteorological parameters such as pressure, temperature and vertical profiles of all absorbers. This has been an important step in adjusting the DOAS algorithm to meet the needs of the near infrared spectral region. However, this approach does not treat different height layers separately, which can result in systematic biases as will be shown in the following. If the actual atmospheric state deviates strongly from the first a priori assumption (e.g. due to the highly variable amount of water vapour or clouds shielding significant parts of the atmosphere), further iterations are necessary in order to yield unbiased results. This can be seen in Fig. 2, where the actual slope of each curve depends on the slant column density S of CH_4, indicating that the sensitivity of the measurement decreases with an increase in the slant column density. Thus, the linearisation point has to be close to the actual state which is only possible by means of iterations. This is of special importance for the retrieval of strongly absorbing gases with highly variable concentrations such as water vapor (see e.g. Buchwitz et Burrows (2004)). A generalised and comprehensive approach to nonlinear and linear inverse problems for atmospheric remote sounding is given by Rodgers (2000).

Given a linearisation point, the derivatives of the measured optical density with respect to perturbations of the respective trace gas columns in different height layers, to temperature changes and other affecting factors can be calculated.

The general concept is a linearisation of the forward model $\mathbf{F}(\mathbf{x})$ at $\mathbf{x_0}$ (nomenclature according to Rodgers (2000):

$$y = F(x_0) + \left. \frac{\partial F(x)}{\partial x} \right|_{x_0} \cdot (x - x_0) + \epsilon \,, \tag{9}$$

where y denotes the measurement $\ln(I/I_0)$ and $F(x_0)$ the theoretical value of $\ln(I/I_0)$ evaluated at a state vector x_0 by means of a radiative transfer model (in the non-scattering case simply the Beer-Lambert law). The state vector comprises the vertical column densities of each absorber as well as deviations from the a priori temperature profile.

The derivatives $\mathbf{K_0} = \left. \frac{\partial F(x)}{\partial x} \right|_{x_0}$ can be represented as a Jacobian Matrix where each column is the derivative vector of the measurement with respect to an element of the state vector. The forward model also has to include the instrumental function which is of special interest in the NIR spectral region.

Thus, we can combine the Beer-Lambert law consisting of a low order polynomial accounting for broadband absorption structures and the instrumental function to obtain the result-

ing simplified forward model, i.e.

$$\frac{I^{lr}}{I_0^{lr}} = <T^{hr}> \,, \tag{10}$$

or with I_0 correction (cf. Aliwell et al. (2002) and Sect. 4.2.1):

$$\frac{I^{lr}}{I_0^{lr}} = \frac{<I_0^{hr} \cdot T^{hr}>}{<I_0^{hr}>} \,, \tag{11}$$

where the indices lr and hr denote low resolution (instrument resolution) and high resolution (resolution high enough to account for all spectral features; for this study we used 0.001 nm). I_0^{hr} is a high resolution Fraunhofer spectrum (in our case taken from Livingston and Wallace, 1991) and T^{hr} the high resolution modeled transmission:

$$T^{hr} = \exp \left(- \sum_j A \cdot \frac{\tau_j^{ref}}{V_j^{ref}} V_j - \sum_k a_k \cdot \lambda^k \right) \,. \tag{12}$$

We can now regard the ratio of the vertical column to be retrieved and the reference vertical column as x^j:

$$x^j = \frac{V_j}{V_j^{ref}} \,. \tag{13}$$

Neglecting the I_0-effect (cf. Sec. 4.2.1), the derivatives of $F(x)$ at x_0 with respect to x^j can be easily deduced:

$$\left. \frac{\partial F(x)}{\partial x^j} \right|_{x_0} = \left. \frac{\partial \ln \left(<T^{hr}(x)> \right)}{\partial x^j} \right|_{x_0}$$

$$= \frac{1}{<T^{hr}(x_0)>} \left. \frac{\partial <T^{hr}(x)>}{\partial x^j} \right|_{x_0}$$

$$= \frac{1}{<T^{hr}(x_0)>} < -T^{hr}(x_0) \cdot A \cdot \tau_i^{ref} > \,. \tag{14}$$

For the computation of the linearisation point, we include an I_0 correction:

$$F(x_0) = \ln \left(\frac{I^{lr}}{I_0^{lr}} \right) = \ln \left(\frac{<I_0^{hr} \cdot T^{hr}(x_0)>}{<I_0^{hr}>} \right) \,. \tag{15}$$

Figures 3a and b show the vertical optical densities τ^{ref} of CH_4 and H_2O at about $2.3\,\mu m$. The derivatives with respect to change in CH_4 column densities in different height layers as well as the derivative with respect to the total vertical column of CH_4 at different VCD's of H_2O are depicted in Figs. 3d and e. It can clearly be seen that the derivatives with respect to CH_4 column density depend on the height at which the actual perturbation takes place. This dependence on height can be readily explained as a result of different mean ambient temperatures and different line-shapes at the respective pressure levels.

Thus, the sensitivity to a perturbation taking place in lower parts of the atmosphere is almost always higher since the
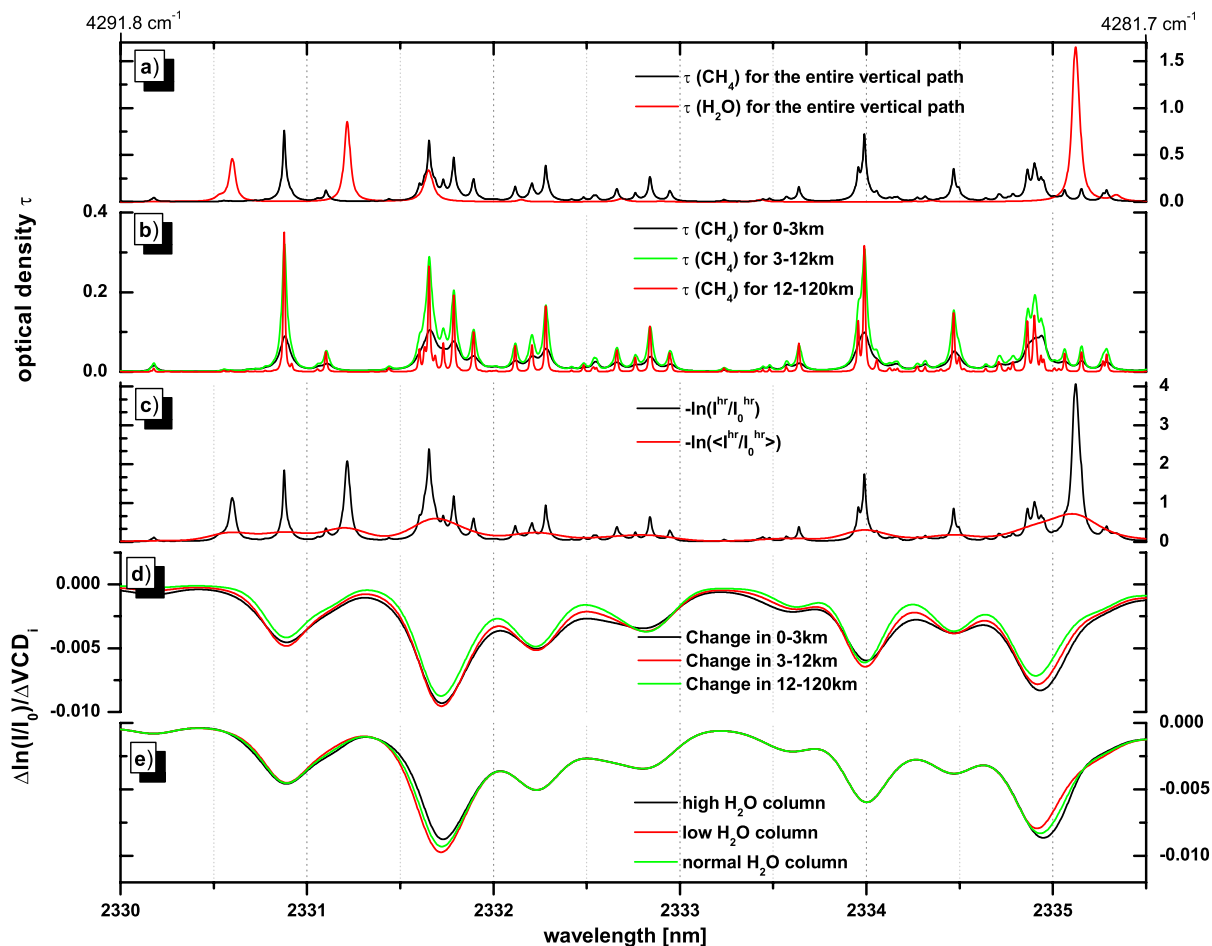
Fig. 3. Panel **(a)** shows the spectrally fully resolved total optical densities for a vertical path for CH_4 ($V=3.6 \cdot 10^{19}$ molec/cm^{-2}) and H_2O ($V=6.5 \cdot 10^{22}$ molec/cm^{-2}) while panel **(b)** depicts the vertical optical densities of CH_4 for different height layers in the atmosphere. The expected total slant optical density (here for $A=2.41$) is now shown in panel **(c)**. Shown is the high resolution optical density and the convolved one that is seen by the instrument, i.e. convolved with ϕ_I (here: SCIAMACHY slit function in channel 8: Gaussian, FWHM=0.24 nm). Starting from this linearisation point, the effect of a change in the vertical column density of CH_4 of $+10^{18}$ molec/cm^2 (i.e. $\approx$3% of the total column) in different height layers is shown in panel **(d)**. Panel **(e)** shows the derivatives (also with respect to CH_4 perturbations) for different linearisation points, viz. for different water vapour columns (1.3, 6.5 and 32.5$\cdot10^{22}$ molec/cm^{-2}, respectively). The optical densities in (a) and (b) are not convolved.

pressure broadened line wings contribute most to the sensitivity. The opposite holds for upper parts of the atmosphere where rather narrow lines exhibit less sensitivity. However, this effect strongly depends on the actual optical density and the slit function of the instrument. The high sensitivity close to the surface can be seen as an advantage, since the boundary layer is of special importance for atmospheric chemistry and atmosphere-geosphere exchange processes.

Interestingly, Fig. 3e shows that the derivatives also depend on the amount of water vapour present. In the case of direct overlapping of the absorption lines, this is obvious because it increases the degree of saturation, and thereby reducing the sensitivity (e.g. at about 2331.75 nm). However, even distinct absorption lines can influence each other if they are close enough to lie within the width of the instrumental function. This can be seen, for instance, at about 2335 nm where enhanced water vapour increases the sensitivity with respect to CH_4 perturbations. In principle, this effect is similar to the well known I_0 effect (Aliwell et al., 2002) differing in that the interfering strong absorption lines are not constant as in case of Fraunhofer lines. This implies that different absorbers cannot be treated separately any more as in the classical DOAS approach.

All these effects are due to the following inequality with respect to convolution:

$$< \boldsymbol{I}_0 \cdot e^{-\tau_a} \cdot e^{-\tau_b} > \neq < \boldsymbol{I}_0 > \cdot < e^{-\tau_a} > \cdot < e^{-\tau_b} > \quad (16)$$

2.4.1 Implementation of Optimal Estimation

We have seen that we are dealing with a nonlinear problem, i.e. the derivatives of the forward model with respect to the column densities of strong absorbers depend on the actual state. Thus, we need an iterative scheme for retrieving the state vector. Further constraints are also necessary since we are dealing with moderate spectral resolution and thus the derivatives at different height layers for the same species are nearly linearly dependent. Thus, the information content of the measurement is not high enough to discriminate between different height layers. In our case, the linear system of equations would be badly conditioned and necessary constraints have to be introduced by the covariance matrix $\mathbf{S}_a$, i.e. by the expected covariances of the a priori state vector before any measurement has been made. Assuming the elements of the state vector to have gaussian distributions, the state vector maximising the a posteriori probability density function of a nonlinear problem can then be written by means of Newtonian iteration (Rodgers, 2000)

$$x_{i+1} = x_a + \left(\mathbf{K}_i^T \mathbf{S}_\epsilon^{-1} \mathbf{K}_i + \mathbf{S}_a^{-1} \right)^{-1} \mathbf{K}_i^T \mathbf{S}_\epsilon^{-1}$$
$$\cdot \left[y - F(x_i) + \mathbf{K}_i (x_i - x_a) \right] , \tag{17}$$

where

x_a	=	a priori state vector ,
x_i	=	state vector at the i-th iteration ,
$\mathbf{S}_\epsilon$	=	(pixel) error covariance matrix ,
$\mathbf{S}_a$	=	a priori covariance matrix ,
$F(x_i)$	=	forward model evaluated at $\mathbf{x}_i$,
$\mathbf{K}_i$	=	Jacobian of the forward model at x_i .

In this paper, optimal estimation according to (17) is applied with a state vector that is comprised of the scaling factors for the vertical columns of the respective trace gases in different height layers, a climatological index for temperature change in the atmosphere (see next Section) and polynomial coefficients accounting for low frequency absorptions and scattering. In the following, this implementation of optimal estimation is referred to as IMAP-DOAS (iterative maximum a posteriori DOAS). Shift and squeeze, a procedure often used in DOAS to account for any slight spectral mismatch between the expected and the actual wavelengths attributed to each detector pixel, can also be easily implemented in this scheme. The Jacobian matrix $\mathbf{K}_i$ is evaluated in each iteration i by computing T^{hr} with $\mathbf{x}_{i-1}$ as input values. At every iteration, several convolutions are involved. Since the numerical computation of a convolution is rather time consuming, neat and fast methods are indispensable. Fast Fourier Transform can in general be used to perform a fast convolution with all kinds of slit functions (Press et al., 2002). Multi-grid binomial filters further decrease the computation time for slit functions having Gaussian shape (cf. Jähne (2002) and references therein).

Allowing only for small variances in $\mathbf{S}_a$ for the scaling factors of the VCD's of higher atmospheric layers, the fit can be constrained to changes in the lower atmosphere where the variance is expected to be high. In case of long lived trace gases like CO_2, this is a reasonable assumption since the stratospheric variations are negligible. $\mathbf{S}_\epsilon$ is usually a diagonal matrix whose elements represents the expected errors (variances, e.g. due to shot-noise or uncertainties in the dark current) of $\mathbf{y}$. Each diagonal element of $\mathbf{S}_\epsilon$ shows a different value, since the variance (in the intensity space) of a particular detector pixel depends on the intensity itself (for shot-noise) transformed via the logarithm (Jähne, 2002). Especially in the near infrared the uncertainties of the dark current can also vary from pixel to pixel which can be accounted for in a proper choice of $\mathbf{S}_\epsilon$.
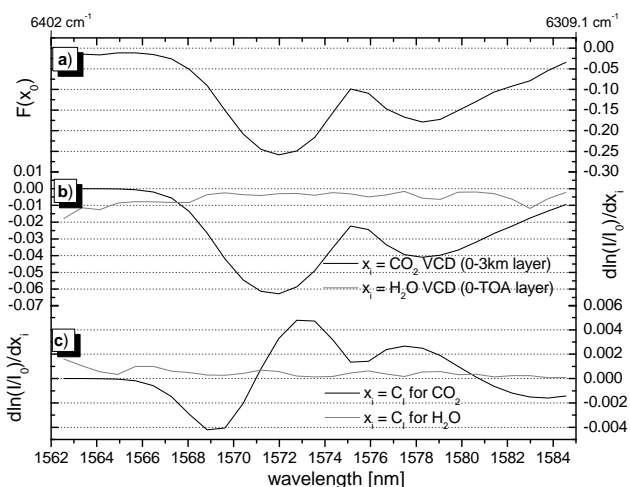
2.4.2 Temperature derivatives

Since the temperature determines the population of the lower state of each transition, the optical densities also depend on temperature, which therefore has to be taken into account. The temperature derivative can be chosen as the derivative of $F(x)$ with respect to temperature. Theoretically, we would have to consider these derivatives for each height layer separately but this would lead to an under-determined linear system of equations. Buchwitz et al. (2000) computed this derivative by assuming a constant temperature change at all height layers. For our study, we choose the temperature difference at each height layer to correspond to a typical difference between two distinct climatologies. This means that we compute the difference quotient $\Delta F(x)/\Delta(T, p)$, where $\Delta(T, p)$ is chosen to correspond to the differences between both climatologies. This method is used throughout this study. $\Delta(T, p)$ can be regarded as the deviation of the pressure and temperature profile from the a priori climatology toward another climatological standard profile, e.g. a deviation from the US standard atmosphere toward a standard mid-latitude winter climatology.

Using this method allows not only for different temperature changes in each height layer, but also changes in the scale height of the atmosphere. $\Delta(T, p)$ can be scaled by a scalar entity C_I (here climatological index). The climatological indices are then part of the state vector and the derivatives are computed for each strong absorber separately, water vapour almost always exhibiting the strongest sensitivity to temperature change. Since water vapour content is highly variable, the temperature (or climatological) derivative should not be directly coupled to, e.g., the temperature derivative of CH_4 or CO_2. However, a covariance of these elements can be assumed and represented in $\mathbf{S}_a$.

The derivative with respect to a climatological index can be computed as the difference of the vertical optical densities of each absorber for different climatologies (the VCD has, of course, to be scaled to a common value), e.g.

$$\Delta \tau_i = \tau_i^{clima_1} - \tau_i^{clima2} \tag{18}$$

Fig. 4. Example of $\mathbf{F}(\mathbf{x_0})$ and temperature derivatives (SZA=60°, $V(CO_2)$=7.75·10^{21} molec/cm^{-2}, $V(H_2O)$=6.5·10^{22} molec/cm^{-2}) for a typical SCIAMACHY CO_2 retrieval with poor spectral resolution (FWHM=1.33 nm).

Here, we have chosen the difference between the US standard atmosphere (a priori climatology) and a mid-latitude winter atmosphere (profiles taken from Kneizys et al., 1996). If scattering is ignored, the derivative can be written analytically as

$$\frac{\partial \mathbf{F}(\mathbf{x})}{\partial C_I} = \frac{1}{<\mathbf{T}^{hr}>} \frac{\partial <\mathbf{T}^{hr}>}{\partial C_I}$$

$$= \frac{1}{<\mathbf{T}^{hr}>} < -\mathbf{T}^{hr} \cdot A \cdot \Delta \boldsymbol{\tau}_i > .$$

Even though this method presumes linear sensitivity with respect to perturbations in the actual pressure/temperature profile, it turned out to yield reasonably precise results.

If computational time were not an issue, vertical optical densities could be computed for each scan using more realistic temperature and pressure profiles, for instance from actual meteorological forecasts or infrared sounders. However, computation of the optical densities is still considerably time consuming, due to which such an approach would not be feasible for the analysis of millions of spectra. Fig. 4, for example, shows $\mathbf{F}(\mathbf{x_0})$ (i.e. the expected $\ln(<\boldsymbol{I}/\boldsymbol{I}_0>)$) in panel (a) and the derivatives of $\mathbf{F}(\mathbf{x_0})$ with respect to perturbation in the CO_2 and H_2O columns in panel (b). Panel (c) depicts the derivative with respect to a change in climatology, separately for CO_2 and H_2O. One can clearly see that this derivative for CO_2 leads to reduced as well as enhanced optical densities in different spectral regions. This facilitates the discrimination of a change in total column from a temperature change.
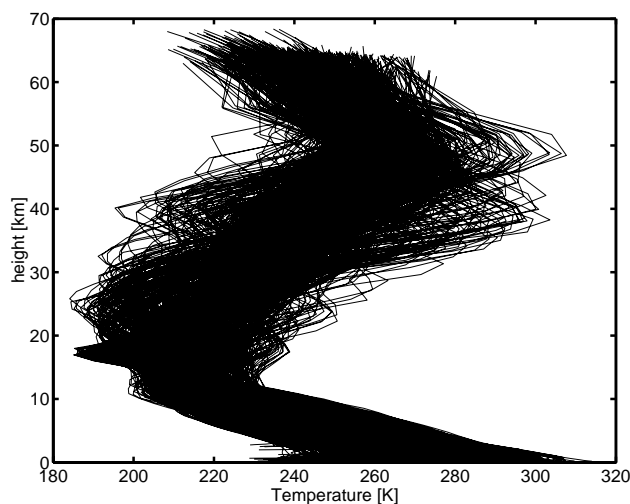
Fig. 5. Range of ECMWF temperature profiles used for the simulation of the retrieval.

3 Simulated retrieval

3.1 Standard profiles

In order to analyze the effect of atmospheric pressure and temperature variability on the retrieval, a comprehensive set of 2000 (for the CH_4 retrieval) and 5000 (for CO_2) ECMWF vertical profiles of temperature (see Fig. 5), pressure and water vapour (Chevallier, 2001) was used to compute optical densities of the absorbers of interest. For CO_2 and CH_4 the profiles were taken from Kneizys et al. (1996) and scaled to actual mixing ratios (tropospheric mixing ratios of 370 ppm for CO_2 and 1.7 ppm for CH_4, corresponding to vertical column densities of 7.75·10^{21} and 3.6·10^{19}, respectively).

Starting from these optical densities, theoretical measurements of $\ln(\boldsymbol{I}/\boldsymbol{I}_0)$ with the spectral resolution of SCIA-MACHY were simulated (scattering as well as instrumental noise were neglected and a solar zenith angle of 45° was chosen). These simulated measurements then were used as input parameters for different versions of the retrieval algorithm. Since the set of profiles also includes surface elevation and was chosen especially to cover a wide range of possible atmospheric states, a comprehensive and realistic simulation could be performed.

The following retrieval schemes were used for the simulation:

a1. For all species of interest, the vertical column density of the entire atmosphere was used in the state vector. Thus, the whole column was scaled with a single factor without accounting for where the change actually takes place. No temperature derivative was included in the state vector. Thus, the state vector only included the total vertical columns of each absorber.

Table 1. Fit windows used for the ECMWF simulated retrieval.

	FWHM [nm]	spectral range [nm]	SZA [°]
CH_4	0.24	2261–2277	45
CO_2	1.3	1562–1585	45

a2. Same as a1) but a climatological index CI accounting for changes in temperature was introduced (U.S. standard atmosphere – mid-latitude winter, cf. Sect. 2.4.2) as an additional entry in the state vector.

b. A full IMAP fit was used: the state vector comprises a climatological index as well as VCD's of strong absorbers divided into different height layers (as an example we chose 3 layers, viz. 0–3 km, 3–12 km, 12–120 km). The fit was confined to the lowermost layer (0–3 km) by setting the variance of higher layers close to zero.

Table 1 shows the fit windows for CO_2 and CH_4 chosen to represent very different instrumental resolutions (given as Full Width at Half Maximum FWHM of the slit function).

For all retrievals, the a priori temperature and pressure profile was the US-standard atmosphere with trace gas concentrations scaled to current values. No surface elevation was included, i.e. the surface pressure was 1013 hPa.
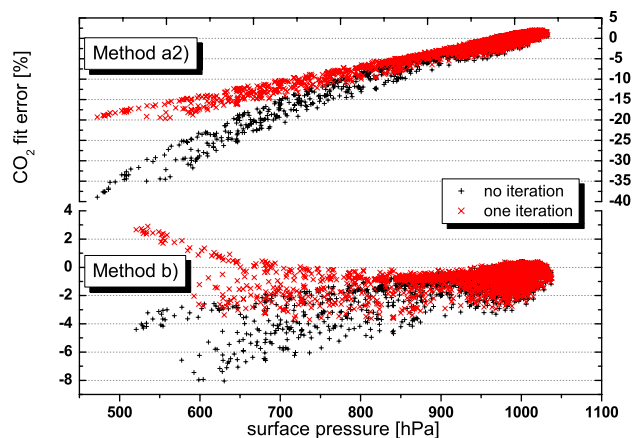
3.1.1 Retrieval results

Figure 6 shows the theoretical errors of a methane fit in a typical SCIAMACHY fit window (see Table 1) plotted against the actual surface pressure. The error is given as the percentage deviation from the true vertical column density $\Delta V_{rel} = \frac{V_{meas} - V_{true}}{V_{true}} \cdot 100\%$. The upper panel shows a retrieval which does not include a temperature derivative in the fit. It can be clearly seen that the errors are far larger than desired for longlived trace gases although only ECMWF profiles within a latitude band between $-60°$ to $-45°$ were considered. The errors for latitudes above $-45°$ were slightly larger. Thus, a derivative of the forward model with respect to temperature is indispensable if high precision is desired. Having analysed a small sample of climatological profiles, Buchwitz et al. (2000) also came to the conclusion that this derivative has to be included in most cases.

The fit window should be chosen such that the absorption lines exhibit a wide variety of lower state energies and thus different responses to temperature changes. In this case, a change in temperature can be well distinguished from an actual change in concentration. Another solution would be to choose only absorption lines with a negligible temperature dependence.

Water vapour, in general, poses a more severe problem due to the predominantly higher values of the lower state ener-
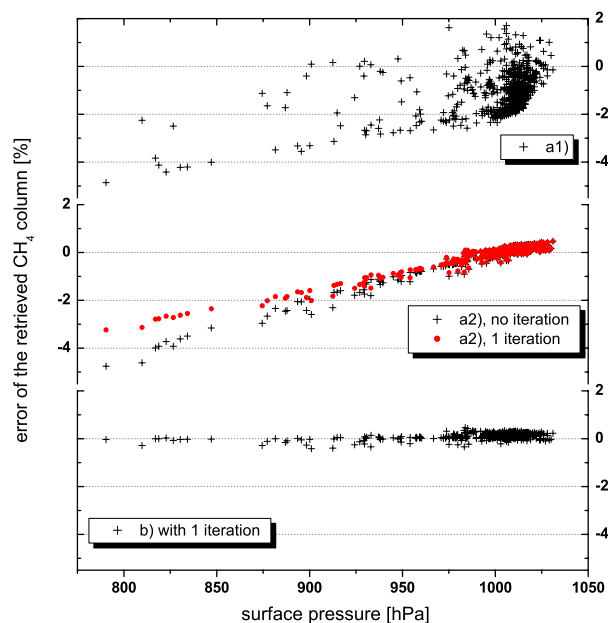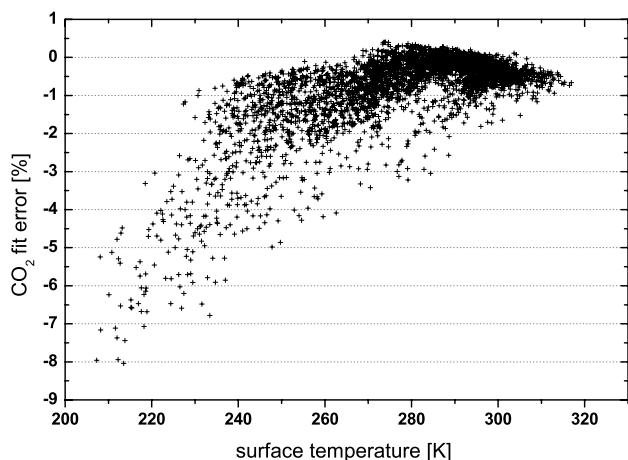

Fig. 6. Error of the retrieved CH_4 vertical column for different ECMWF profiles and retrieval methods (see text for the explanation of **a1**, **a2** and **b**) in a latitude band of $-60°$ to $45°$. Only method (b) avoids huge errors due the atmospheric variability of temperature and pressure (dominant in a1) and the systematic bias dominant in a2.

Fig. 7. Error of the retrieved CO_2 vertical column for different ECMWF profiles. Please note the different scale for both panels. A second iteration would yield nearly identical results as using only one iteration for both algorithms.

gies, which implies a stronger temperature dependence of the absorption line. Furthermore, the actual water vapour profile can vary considerably and thus vary in concentration in layers of different sensitivities inducing systematic errors. This could be of great significance in, e.g., a precise water vapour retrieval with moderate spectral resolution where no height information can be extracted from the spectra.

Fig. 8. Error of the retrieved CO_2 vertical column for different ECMWF profiles with respect to surface temperature. Profiles with a surface elevation of more than 200 m have been excluded.

Fig. 9. Error of the retrieved CO_2 vertical column for different ECMWF profiles with and without enhancement of 50 ppm CO_2 in the lowermost kilometer. Profiles with a surface elevation higher than 200 m and a surface temperature lower than 270 K have been discarded.

Also, it can be seen that scaling the entire column (method a2) creates an artificial bias in the retrieved column and would lead to averaging kernels above unity in the lower parts of the atmosphere. As mentioned before, this problem can be alleviated by including surface elevation in the a priori (i.e. when the a priori optical density is not computed from $z=0$ to the top of atmosphere but from $z=$surface elevation to the top of atmosphere). On the other hand, the nonlinearity is also not negligible on scales of actual meteorological surface pressure changes ($\pm\approx30$ hPa). Confining the fit to the lower atmosphere circumvents these problems, since it properly accounts for the higher sensitivity to the boundary layer. In order to account for, for instance, seasonal changes in CO_2 column which occur throughout the troposphere, the fit could be extended to encompass the entire troposphere (e.g. by using a height layer of 0–10 km instead of only 0–3 km or by setting higher variances in $\mathbf{S_a}$ for height layers above 3 km and below 10 km).

As already pointed out, the impact of nonlinearity becomes substantial when either the actual state deviates strongly from the a priori state (e.g. when clouds shield most parts of the lower atmosphere or mountains are present) or the state vector is not properly chosen (e.g. scaling the whole column instead of only the lower atmosphere). Figure 7 underlines this effect in several ways: Without iteration, an additional bias is introduced at low surface pressures. This effect could be only partly obviated by a more accurate a priori estimation of the surface pressure (e.g. an elevation database). Moreover, scaling the entire column creates an artificial bias of up to 20% because the actual change in concentration takes place in the lower atmosphere whereas the fit algorithm scales the whole column. The slope of this bias depends on the degree of saturation, and thereby also on the slit function and the air mass factor.
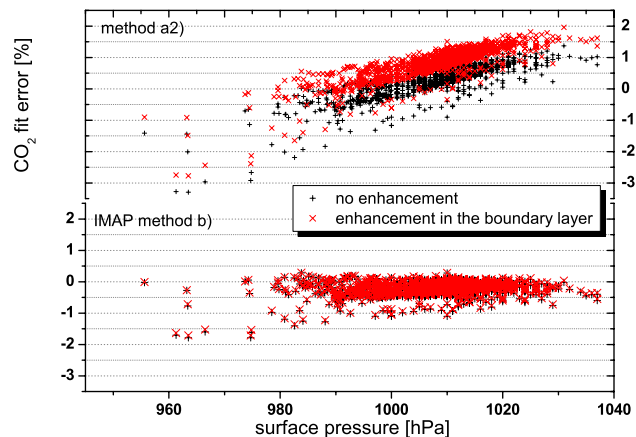
To summarise, it can be said that Fig. 7 shows two different types of biases, one induced by different sensitivities in different height layers (the slope of the upper panel using one iteration, avoided by the IMAP-DOAS algorithm in the lower panel), and the other induced by the general nonlinearity of the problem (see curve of growth in Fig. 2), which explains the differences of both methods using no and one iteration. Furthermore, it reveals a source of error, namely the uncertainty in pressure and temperature profiles leading to a scatter of up to 1–2% of the retrieved column.

The IMAP algorithm in the lower panel (using one iteration) starts to overestimate the total column when the surface pressure drops below values corresponding to a height of 3km since the height layer between 0–3 km has been used as entry in the state vector (which does not exist any more since this layer has been clipped by mountains). This is prevented by supplying a priori information about the surface elevation, e.g. by setting the lower level of the lowest height layer to the actual surface elevation.

Figure 8 shows that the errors caused by the IMAP fit increase with decreasing surface temperature. This is mainly because the a priori has been based on the US-standard atmosphere. In most cases, this is a fair approximation, in extremely cold atmospheres, though, a more appropriate a priori profile needs to be adopted in order to yield more precise results.

3.2 Simulating enhanced CO_2 in the boundary layer

The short term variability of longlived trace gases is expected to be highest in the boundary layer, close to the surface where the sources and sinks (Olsen and Randerson, 2004) are located. If the algorithm does not properly account for this additional information, the retrieved column will be biased.

To quantify this effect, artificial measurements (see Sect. 3.1) with an enhancement of 50 ppm CO_2 in a boundary layer of 1 km vertical extent have been simulated and retrieved by different algorithms. The results of two methods, viz. a2 and b, are depicted in Fig. 9. Using method a2, the bias produced receives an additional offset of about 0.6% while the IMAP-DOAS algorithm remains unaffected by this change in concentration profile (lower panel).

4 Other parameters influencing the retrieval

4.1 Radiative transfer

4.1.1 Effect of atmospheric scattering

In the near infrared spectral region, Rayleigh scattering is nearly negligible and plays only a minor role. However, aerosols and clouds can significantly alter the distribution of the light paths. Thick clouds alter the light path dramatically and often render measurements useless. However, they are far easier to detect than aerosols or thin cirrus clouds, serving to generate a mask according to which measurements can be discarded. As O'Brien and Rayner (2002) pointed out, also thin cirrus can significantly shorten the light path, thus also biasing the retrieved column by up to a few percent. Depending on their optical properties, surface reflectance and other parameters, aerosols can shorten as well as enhance the light path by up to a few percent (see e.g. O'Brien and Rayner (2002), Dufour and Breon (2003) or Buchwitz et Burrows (2004)). To alleviate the difficulties posed by these factors in the estimation of the actual light path distribution, O_2 can be used as a proxy for the light path distribution (Pfeilsticker et al., 1998; Pfeilsticker, 1999). O'Brien and Rayner (2002) proposed the nearby 1.27 μm region for the retrieval of O_2 since the scattering properties of the spectral retrieval window of the proxy species have to be as similar as possible to that of the retrieval windows of the target species.

Using a proxy for the light path primarily requires an unbiased spectral analysis of both species, e.g. O_2 and CO_2. Being outside the scope of this paper, a comprehensive analysis of the influence of single and multiple scattering will not be given. It should be mentioned that especially the O_2 A-band at 765 nm which is often used for the determination of airmass factors, exhibits very strong absorptions, thus also strong height-dependence of the sensitivity. Neglecting the issues addressed in this paper would lead to systematic biases in the retrieved airmass factor and subsequently also in the target species.

4.1.2 Effect of surface elevation and albedo

When the footprint of a measurement is relatively coarse (e.g. 30×60 km for SCIAMACHY), cross-correlations between the surface altitude and surface albedo can introduce systematic errors. If, for instance, 50% of the ground pixel has a height of 500 m and an albedo of 0.02 and the other 50% a height of 200 m and an albedo of 0.2, the systematic error would be about 1.5% in the total column (for an nearly equally distributed gas such as CH_4 or CO_2). Especially snow covered areas above a certain altitude with a low albedo in the NIR can create cross-correlations between the surface altitude and albedo.

One could use broadband measurements with a finer spatial resolution to provide a more accurate weighting for different areas of a given ground-pixel or exclude pixels with a surface altitude variance higher than a predefined threshold. SCIAMACHY provides broadband detectors having higher spatial resolution that can be used to derive this information. In using proxies such as O_2, care has to be taken that the albedos for the O_2 retrieval are similar to the retrieval window used for, e.g., CO_2.

4.2 Spectroscopical aspects

4.2.1 I_0 effect

Although the density of the Fraunhofer lines in the near infrared is not as pronounced as in the UV/Vis, the spectral structure of the incoming solar radiation I_0 and their undersampling may introduce errors (Aliwell et al., 2002). This effect is similar to the effect of overlapping strong absorbers as in Fig. 3d. The I_0 corrected slant optical density can be written as

$$\tau_\lambda^{corr}(x) = -\ln\left(\frac{<I_0\exp(-x\cdot A\cdot\tau_\lambda^{ref})>}{<I_0>}\right). \qquad (19)$$

The I_0 effect is implemented in the evaluation of the forward model $F(x)$ and is thus properly corrected. The highly resolved solar atlas used in this study was obtained from Livingston and Wallace (1991).

As can be seen in Fig. 10, the I_0 effect can have a relatively strong influence on the slant optical densities. Especially the absorption bands at about 1575 nm that are used for CO_2 retrieval from SCIAMACHY show a strong effect.

4.2.2 Effect of the uncertainty of broadening parameters

As already stated, the actual shapes of the absorption lines are important for the retrieval of strong absorbers. Thus, if the broadening coefficients are larger than given in the literature, the sensitivity of $\ln(I/I_0)$ with respect to concentration changes of the respective absorber will be underestimated and vice versa. This is due to the reduced degree of saturation of broader lines. However, wrong broadening parameters not only introduce systematic errors in the total columns of strong absorbers but also systematic residuals in the fit which can become stronger than spectral structures of some weak absorbers of interest.

According to Rothman et al. (2003), the effective pressure broadened halfwidth $\gamma_L(p,T)$ of a molecule with a partial
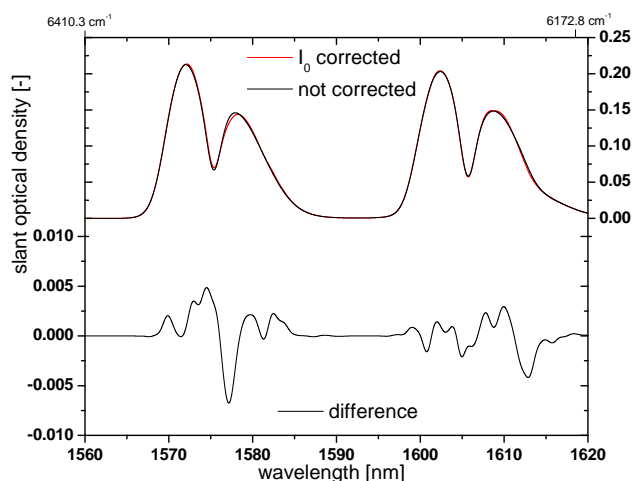
Fig. 10. Slant optical densities of CO_2 with and without I_0 correction (AMF=3, FWHM=1.3 nm). The lower panel shows the difference of the I_0 corrected and the uncorrected slant optical density.
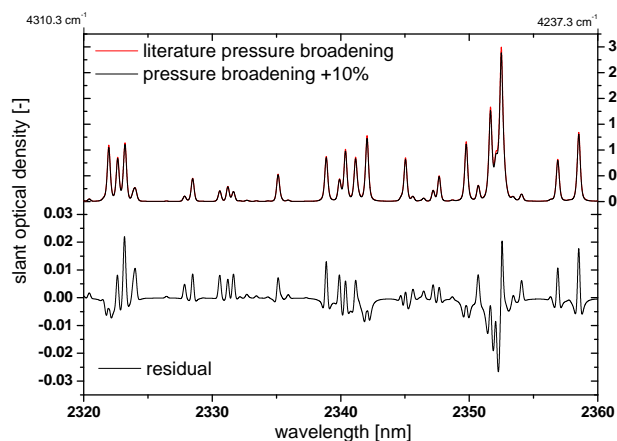
Fig. 11. Influence of the pressure broadening coefficient γ_L^{air} on the apparent differential slant optical densities of H_2O. The remaining residual of a linear fit of both is shown in the lower panel.

pressure far lower than the actual pressure p [atm] is calculated as

$$\gamma_L(p, T) = \left(\frac{T_{ref}}{T}\right)^n \gamma_L^{air}(p_{ref}, T_{ref}) \cdot p , \qquad (20)$$

where n is the coefficient of temperature dependence of γ_L. Especially for water vapour the line parameters exhibit large uncertainties and the absorptions in many areas in the near infrared are very strong (optical density in the line centre > 10).

Figure 11 shows the effect of a change of 10% in γ_L^{air} for H_2O at US standard atmosphere concentrations and an air mass factor of 3 (corresponding to a solar zenith angle of 60°). The upper panel depicts the two optical densities at SCIAMACHY resolution (FWHM=0.24 nm) for the same vertical column density. If the actual value of γ_L^{air} would be

10% higher than expected, the total column would be overestimated by approximately 4%. It would also introduce a stable residual which is shown in the lower panel of Fig. 11. Washenfelder et al. (2003), for instance, found wrong broadening parameters for CH_4 at about 1680 nm which lies in a wavelength region of special importance for the CH_4 retrieval with SCIAMACHY.

Since the influence of an error in γ_L^{air} depends on the strength of the absorption lines, it also depends on the solar zenith angle. Thus, the systematic bias introduced by a wrong value of γ_L^{air} also depends on the solar zenith angle. Hence, a simple correction factor cannot be applied.

4.2.3 Effect of the uncertainty of the slit function

Since the slit function mainly determines the sensitivity and the nonlinearity of the measurement (see Fig. 2), errors can be introduced if the slit function is incorrectly specified. We analysed this effect on a rather simple example, viz. the effect of a change of the FWHM of a gaussian slit function on the CH_4 retrieval at about 2270 nm. If the true FWHM deviates by 0.02 nm from the assumed one (0.24 nm), the errors in the retrieved CH_4 columns are +3.1% and −2.6%, respectively for a true FWHM of 0.22 and 0.26 nm. This error varies only slightly (0.3%) over a large range of air mass factors (2–5).

However, in some cases the actual slit function deviates strongly from the expected one such as in the case of channels 7 and 8 of SCIAMACHY where an ice layer leads to largely extended wings of the slit function. This could give rise to errors in the retrieved columns of up to 25% (Gloudemans et al., 2004). Thus, a precise knowledge of the slit function is indispensable.

5 Conclusions

We have investigated several important aspects that can complicate the spectroscopic analysis of atmospheric trace gases in the presence of strong absorbers. The nonlinearity of the classical DOAS approach in situations where non-resolved lines prevail, e.g. in the near infrared spectral region, was analysed and a new IMAP-DOAS algorithm based on optimal estimation was implemented to account for the peculiarities of this spectral region.

The nonlinearity of the problem requires the use of iterations which are implemented in the IMAP-DOAS algorithm. In the iterative procedure, the vertical column densities are directly fitted such that the total slant optical density of all absorbers matches the measurement. By using convolutions with the instrumental slit function in every iteration, any interference between different absorbers or with the Fraunhofer spectrum that may occur in the classical DOAS approach is resolved. This is of importance in all cases where strong absorbers have to be retrieved (e.g. CO_2, CH_4 or O_2) or when

strong absorbers interfere with the target species to be retrieved (e.g. O_3 interferences with SO_2).

Furthermore, we showed that for strong absorbers in the near infrared, the sensitivity of $\ln(I^{lr}/I_0^{lr})$ with respect to perturbations in concentration mostly increases with increasing ambient pressure due to pressure broadening of the absorption lines. This effect can lead to a strong systematic bias, if the whole atmosphere is scaled with a single factor as is often done in conventional DOAS algorithms. The IMAP-DOAS method circumvents this problem by confining the fit to the lowermost layers of the atmosphere.

The analysis also shows that a further derivative for changes in the temperature profile is indispensable. In Absence of this derivative, errors of up to several percent in the total column may arise.

Although spectrometers with moderate spectral resolution cannot fully resolve the absorption lines, it has been shown that the actual lineshape is of special importance since it determines the sensitivity of the measurement. Thus, an accurate knowledge of the lineshape, especially the broadening parameters, is necessary to avoid further biases.

The techniques elaborated in this paper are applicable to all cases where non-resolved strong spectral structures are encountered. Some error sources still remain: uncertainties in the light-path due to aerosols, inhomogeneous surface elevation or partial cloud cover giving rise to errors of a few percent that can only be circumvented by using a suitable proxy. Incorrect specification of the instrumental slit function can lead to a rather constant bias of 1–5%, in extreme cases of up to 25%. Using a climatological derivative, the errors induced by perturbations in the temperature and pressure profile can be reduced to mostly below 1%.

References

Aliwell, S., Johnston, P., Richter, A., Roozendael, M. V., Wagner, T., Arlander, D., Burrows, J., Fish, D., Jones, R., Tørnkvist, K. K., Lambert, J.-C., Pfeilsticker, K., and Pundt, I.: Analysis for BrO in zenith-sky spectra: An intercomparison exercise for analysis improvement, J. Geophys. Res., 107, 4199, doi:10.1029/2001JD000329, 2002.

Bovensmann, H., Burrows, J. P., Buchwitz, M., Frerik, J., Noël, S., Rozanov, V. V., Chance, K. V., and Goede, A.: SCIAMACHY – mission objectives and measurement modes, J. Atmos. Sci., 56, 127–150, 1999.

Buchwitz, M., Rozanov, V., and Burrows, J.: A near-infrared optimized DOAS method for the fast global retrieval of atmospheric CH_4, CO, CO_2, H_2O, and N_2O total column amounts from SCIAMACHY Envisat-1 nadir radiances, J. Geophys. Res., 105, 15 231–15 245, 2000.

Buchwitz, M. , de Beek, R. ,Bramstedt, K. , Noël, S. , Bovensmann, H., and Burrows, J.: Global carbon monoxide as retrieved from SCIAMACHY by WFM-DOAS, Atmos. Chem. Phys., 4, 1945–1960, 2004,
SRef-ID: 1680-7324/acp/2004-4-1945.

Buchwitz, M., de Beek, R., Burrows, J. P., Bovensmann, H., Warneke, T., Notholt, J., Meirink, J. F., Goede, A. P. H., Bergamaschi, P., Körner, S., Heimann, M., Müller, J. F., and Schulz, A.: Atmospheric methane and carbon dioxide from SCIAMACHY satellite data: Initial comparison with chemistry and transport models , Atmos. Chem. Phys. Discuss., 4, 7217–7279, 2004,
SRef-ID: 1680-7375/acpd/2004-4-7217

Buchwitz, M. and Burrows, J. P.: Retrieval of CH_4, CO, and CO_2 total column amounts from SCIAMACHY near-infrared spectra: Retrieval algorithm and first results, Proceedings of SPIE 5235, Remote Sensing of Clouds and the Atmosphere VII, edited by: Schäfer, K. P., Comeron, A., Carleer, M. R., and Picard, R. H., 375–388, 2004.

Chevallier, F.: Sampled databases of 60-level atmospheric profiles from the ECMWF analyses, Research. rep. no. 4, EUMETSAT/ECMWF, http://www.metoffice.com/research/interproj/nwpsaf/rtm/, 2001.

Clough, S., Kneizys, F., and Davies, R.: Line Shape and the Water Vapor continuum, Atmos. Res., 23, 229–241, 1989.

Dufour, E. and Breon, F.M.: Spaceborne estimate of atmospheric CO_2 column bz use of the differentil absorption method: error analysis, Appl. Opt., 42, 3595–3609, 2003.

Gloudemans, A., Schrijver, H., Straume, A., Aben, I., Maurellis, A., Buchwitz, M., de Beek, R., Frankenberg, C., and Wagner, T.: CH_4 and CO total columns from SCIAMACHY: comparisons with TM3 and MOPITT, in: Proc. ACVE2, 3–7 May, Frascati, Italy, 2004.

Goody, R. and Yung, Y.: Atmospheric Radiation, Oxford University Press, New York, 1989.

Jähne, B.: Digital Image Processing, Springer, Berlin, 5th edn., 2002.

Kneizys, F. X., Abreu, L. W., Anderson, G. P., Chetwynd, J. H., Shettle, E. P., Robertson, D. C., Acharya, P., Rothman, L., Selby, J. E. A., Gallery, W. O., and Clough, S. A.: The MODTRAN 2/3 report and LOWTRAN 7 model, Tech. rep., Phillips Laboratory, Geophysics Directorate, Hanscom AFB, 1996.

Kuntz, M.: A new implementation of the Humlíček algorithm for the calculation of the Voigt profile function, J. Quant. Spectrosc. Radiat. Transfer, 57, 819–824, 1997.

Levin, I., Ciais, P., Langenfelds, R., Schmidt, M., Ramonet, M., Sidorov, K., Tchebakova, N., Gloor, M., Heimann, M., Schulze, E., Vygodskaya, N., Shibistova, O., and Lloyd, J.: Three years of trace gas observations over the EuroSiberian domain derived from aircraft sampling – a concerted action, Tellus, 54B, 696–712, 2002.

Livingston, W. and Wallace, L.: An Atlas of the Solar Spectrum in the Infrared from 1850 to 9000 cm^{-1} (1.1 to 5.4 μm), Tech. rep. 91–001, National Solar Observatory, 1991.

Ma, Q. and Tipping, R.: The averaged density matrix in the coordinate representation: Application to the calculation of the far-wing line shapes for H_2O, J. Comp. Phys., 111, 5909, 1999.

Maurellis, A., Lang, R., and van der Zande, W.: A New DOAS Parameterization for Retrieval of Trace Gases with Highly-Structured Absorption Spectra, Geophys. Res. Lett., 27, 4069–4072, 2000.

O'Brien, D. M. and Rayner, P. J.: Global observations of the carbon budget, 2. CO_2 column from differential absorption of reflected sunlight in the 1.61 μm band of CO_2, J. Geophys. Res., 107, 4354, 2002.

Olsen, S. C. and Randerson, J. T.: Differences between surface and column atmospheric CO_2 and implications for carbon cycle research, J. Geophys. Res., 109, 2004.

Pfeilsticker, K.: First geometrical path lengths probability density function derivation of the skylight from spectroscopically highly resolving oxygen A-band observations, 2. Derivation of the Levy-index for the skylight transmitted by mid-latitude clouds, J. Geophys. Res., 104, 4101–4116, 1999.

Pfeilsticker, K., Erle, F., Funk, O., Veitel, H., and Platt, U.: First geometrical pathlengths probability density function derivation of the skylight from spectroscopically highly resolving oxygen A-band observations, 1. Measurement technique, atmospheric observations, and model calculations, J. Geophys. Res., 103, 11 483–11 504, 1998.

Pine, A.: N_2 and Ar broadening and line mixing in the P and R branches of the ν_3 band of CH_4, J. Quant. Spectrosc. Radiat. Transfer, 57, 157–176, 1997.

Platt, U.: Differential optical absorption spectroscopy (DOAS), in Air Monitoring by Spectroscopic Techniques, John Wiley, New York, 1994.

Press, W., Teukolsky, S., Vetterling, W., and Flannery, B.: Numerical Recipes in C/C++ – The Art of Scientific Computing, Cambridge University Press, 2002.

Rayner, P. J. and O'Brien, D. M.: The utility of remotely sensed CO_2 concetration data in surface source inversions, Geophys. Res. Lett., 28, 175–178, 2001.

Rayner, P. J., Law, R. M., O'Brien, D. M., Butler, T. M., and Dilley, A. C.: Global observations of the carbon budget, 3, Initial assessment of the impact of satellite orbit, scan geometry, and cloud on measuring CO_2 from space, J. Geophys. Res., 107, 4557, doi:10.1029/2001JD000618, 2002.

Rodgers, C.: Retrieval of atmospheric temperature and composition from remote measurements of thermal radiation, Rev. Geophys. Space Phys., 14, 609–624, 1976.

Rodgers, C. D.: Inverse Methods for Atmospheric Sounding, World Scientific, London, 2000.

Rothman, L., Barbe, A., Benner, D. C., Brown, L., Camy-Peyret, C., Carleer, M., Chance, K., Clerbaux, C., Dana, V., Devi, V., Fayt, A., Flaud, J.-M., Gamache, R., Goldman, A., Jacquemart, D., Jucks, K., Lafferty, W., Mandin, J.-Y., Massie, S., Nemtchinov, V., Newnham, D., Perrin, A., Rinsland, C., Schroeder, J., Smith, K., Smith, M., Tang, K., Toth, R., Auwera, J. V., Varanasi, P., and Yoshino, K.: The HITRAN molecular spectroscopic database: edition of 2000 including updates through 2001, J. Quant. Spectrosc. Radiat. Transfer, 82, 5–44, 2003.

Schrijver, H.: Retrieval of carbon monoxide, methane and nitrous oxide from SCIAMACHY measurements, Proc. ESAMS, European Symposium on Atmospheric Measurements from Space, ESA WPP-161 1, ESTEC, Noordwijk, The Netherlands, 285–294, 1999.

Solomon, S., Miller, H. L., Smith, J. P., Sanders, R. W., Mount, G. H., Schmeltekopf, A. L., and Noxon, J. F.: Atmospheric NO_3, 1. Measurement Technique and the Annual Cycle, J. Geophys. Res, 94, 11 041–11 048, 1989.

Strow, L. and Reuter, D.: Effect of line mixing on atmospheric brightness temperatures near 15 μm, Appl. Opt., 27, 872–878, 1988.

Tans, P., Bakwin, P., and Guenther, D.: A feasible global carbon cycle observing system: a plan to decipher today's carbon cycle based on observations, Global Change Biol., 2, 309–318, 1996.

Thomas, G. E. and Stamnes, K.: Radiative Transfer in the Atmosphere and Ocean, Cambridge University Press, Cambridge, 1999.

Volkamer, R., Etzkorn, T., Geyer, A., and Platt, U.: Correction of the Oxygen Interference with UV Spectroscopic (DOAS) Measurements of Monocyclic Aromatic Hydrocarbons in the Atmosphere, Atmos. Environ., 32, 3731–3747, 1998.

Wagner, T. and Platt, U.: Satellite mapping of enhanced BrO concentrations in the troposphere, Nature, 395, 486–490, 1998.

Washenfelder, R., Wennberg, P., and Toon, G.: Tropospheric methane retrieved from ground-based near-IR solar absorption spectra, Geophys. Res. Lett., 30, 2226, 2003.

Yang, Z., Toon, G. C., Margolis, J. S., and Wennberg, P. O.: Atmospheric CO_2 retrieved from ground-based near IR solar spectra, Geophys. Res. Lett., 29, 1339, 2002.